JCHR (2024) 14(1), 159-166

Journal of Chemical Health Risks

jchr.damghan.iau.ir

ORIGINAL ARTICLE

New Imidazo[4,5-*a*] Acridine: Synthesis and Studying the Molecular Dynamics Simulation of Its Interaction with the Topoisomerase Enzyme

Maryam Rangamiz Toosi, Mehdi Pordel*, Mohammad Reza Bozorgmehr

Department of Chemistry, Mashhad Branch, Islamic Azad University, Mashhad, Iran

(Received: 17 April 2023 Accepted: 9 September 2023)

KEYWORDS

Imidazo[4,5-*a*]acridine;
Molecular modeling;
Aromaticity;
Topoisomerase

ABSTRACT: Acridine and imidazole were combined and synthesized 3,8-disubstituted-propyl-3*H*-imidazo[4,5-*a*]acridine-11-carbonitrile, as a new derivative. The interaction of this new compound with the topoisomerase enzyme was studied by molecular dynamics simulation. The 3,8-disubstituted-3*H*-imidazo[4,5-*a*]acridine-11-carbonitrile structure has been optimized by the density functional theory method. According to the results obtained from the molecular dynamics simulation, Arg364, Lys532, Asp533, Tyr537, Arg590, Cys630, Asn631, Gln633 and Adenine11 interact with the ligand by hydrophobic interactions and Arg488 and Adenine12 interact with the ligand by hydrogen bond interactions. Due to the fact that some of these residues, Arg488 and Arg590 are located in the enzyme active site, the new ligand appears to be inhibitory effect. Also, the calculation of the Harmonic Oscillator Model for Aromaticity (HOMA) index showed that the 5-membered ring of ligand and the 6-membered ring attached to the 5-membered ring had more reactivity with the enzyme. The contribution of charged residues in the binding free energy of the ligand is greater than the uncharged residues.

INTRODUCTION

Acridine scaffolds have a variety of useful pharmacological properties, including anti-inflammatory [1,2], antiviral [3], antimicrobial [4, 5] and anticancer activities [6]. Because of their ability to intercalate into DNA, acridines are used as chemotherapeutic drugs, particularly as antitumor agents, resulting in topoisomerase inhibition [7]. Imidazole derivatives, on the other hand, have emerged as extremely effective bioactive compounds, pharmaceuticals, and synthetic intermediates. They can be found in the primary structure of certain well-known human organism components like the amino acid histidine. Furthermore, these compounds exhibit crucial biological activities including antibacterial activities [8], anti-inflammatory [9], anti-plasmodium [10] as well as antifungal [11, 12].

Eukaryotic topoisomerases recognize DNA topology and preferentially react with positively or negatively super coiled molecules over relaxed substrates. Eukaryotic topoisomerases recognize two properties of their DNA substrates. On the one hand, the type I and II enzymes can discern the topological state of DNA [13].

The catalytic group at topoisomerase I's active site is the hydroxyl side chain of tyrosine residue. This functional group can be a nucleophilic attack on phosphorus, breaking the phosphodiester bond and forming a new phosphodiester connection on the 5′ side of DNA. In the next step, 3′- OH of the broken strand attacks to the phosphodiester bond. Finally, the phosphodiester bond between 3′- OH and 5′-Pi in the DNA nucleotide chain is formed. Some compounds have been shown to

*Corresponding author: mehdi.pordel@iau.ac.ir; mehdipordel58@yahoo.com (M. Pordel)
DOI: 10.22034/jchr.2023.1984058.1724

strengthen this bond. Camptothecin, for example, binds the 3′-phosphotyrosyl intermediate and prevents DNA leligation. Topoisomerase I is thus converted into a DNA-damaging compound [14,15].

In the process of creating cancer cells, the speed of nucleic acid multiplication increases. On the other hand, topoisomerase enzyme increases the speed of reproduction. Therefore, any compound that can limit its activity can be effective in controlling cancer. On the other hand, organic compounds such as acridine have an inhibitory effect on enzymes such as topoisomerase. For this reason, this research was studied with this feature.

Molecular modeling studies are used to investigate the behavior of different enzymes [16]. In this work, acridine and imidazole were combined and synthesized a new imidazo[4,5-*a*] acridine derivative. Also, we investigated the interaction of this new compound with *topo-I* by molecular dynamics simulation.

MATERIALS AND METHODS

Experimental

In accordance with industry standards, all solvents got dryness. Compounds 2 [17] as well as 4 [18] got synthesis following the method of the literatures. Other compounds were purchased from Merck.

On a Varian Mat, CH-7 at 70 Ev, the mass spectra were achieved. The analysis was conducted on a Thermo Finnigan Flash EA microanalyzer. Electrothermal Type-9100 melting-point apparatus was applied to obtain melting points. The IR (as KBr discs) spectra was acquired on a Tensor 27 spectrometer and just notable absorptions are noted. a Bruker Avance DRX-300 spectrometer in DMSO-d_6 was used to record the ^{13}C NMR (75 MHz) and the ^{1}H NMR (300 MHz) spectra. Chemical changes are measured in parts per million downfield from the internal standard, tetramethyl silane (TMS); coupling constant *J* is provided in Hz. All measurements were performed at room temperature.

In an ice-bath at rt, compound 4 (34 mmol) was mixed in while stirring to H_2SO_4 (98%, 30 mL) during a one-hour period. The solution was then agitated at room temperature for an additional 4 hours, and in an ice-bath, water (40 mL) was incorporated into the solution and agitated for another 2 hours before being poured over crushed ice, and finally, dilute aqueous NaOH was used to neutralize it.

Then, the reaction mixture was let on to attain a temperature of 50-70°C. Throughout the neutralization process. When cooled to room temperature, it was filtered and washed with water to produce new compounds 5.

8-Methoxy-3-propyl-3*H*-imidazo[4,5-*a*] acridine-11-carbonitrile (5). Compound 5 was achieved in the form of yellow needles. (EtOH), (70%), m.p.: > 300 °C (decomp.); IR (KBr disk): NH_2 3344, 3327 cm^{-1}, C=O 1687 cm^{-1}; ^{1}H NMR: δ 0.99 (t, 3 H, $CH_2CH_2C\underline{H}_3$, *J* = 7.2 Hz), 1.75–1.95 (m, 2 H, $CH_2C\underline{H}_2CH_3$), 3.96 (s, 3 H, OMe), 4.47 (t, 2 H, $C\underline{H}_2CH_2CH_3$, *J* = 7.2 Hz), 6.41 (s, br, NH), 6.52 (s, br, NH), 7.59 (dd, *J*= 8.8 Hz, J= 2 Hz, 1H, Ar H), 7.8 (d, *J*= 9.2 Hz, 1H, Ar H), 7.95 (d, *J*= 9.2 Hz, 1H, Ar H), 8.09 (d, *J*= 8.8 Hz, 1H, Ar H), 8.2 (d, *J*= 2 Hz, 1H, Ar H), 8.57 (s, 1H, Ar H) ppm; ^{13}C NMR (125 MHz): δ 10.2, 24.5, 39.4, 49.0, 111.5, 112.0, 115.3, 117.1, 119.5, 122.5, 122.7, 123.9, 129.4, 130.6, 131.7, 138.8, 141.0, 146.6, 165.3 ppm; MS (EI, 70 eV), *m/z* (I_{rel} (%)): 334 $[M]^+$ (7). Found: C, 68.47; H, 5.46; N, 16.59. $C_{19}H_{18}N_4O_2$ (334.4) Calculated (%): C, 68.25; H, 5.43; N, 16.76.

Simulation details

The Human topoisomerase type I with the code 1A36 in the protein data bank was put at the simulation box's middle [19,20]. According to the procedure described by Chillemi et al., *Topo-I* structure is anywise provided such that pH becomes neutral [21,22]. In order for this goal, Lysine and Arginine got protonation and Aspartate and Glutamate got deprotonation. For Histidine, Half of the sample was protonated, while the other half was deprotonated. Then, five molecules were added to simulation box. The *Topo-I* was placed in the center of the box and the 5 molecules were randomly placed. The designed box is filled with water type TIP3P. All molecular dynamics simulations were carried out using the Gromacs package version 5.1.2 and Charm27 all atom force field.

As the force field settings for 5 are not provided in the Gromacs software's default version, using of B3LYP with primary function of 6-31G*, the compound's structure has been optimized. B3LYP model is used in

many researches [23]. Frequency calculations were done to regulate the optimization and virtual frequencies were not noticed. GAMESS software was used to do all ab initio computations [24, 25]. Figure 1 depicts the optimal structure of the 5.

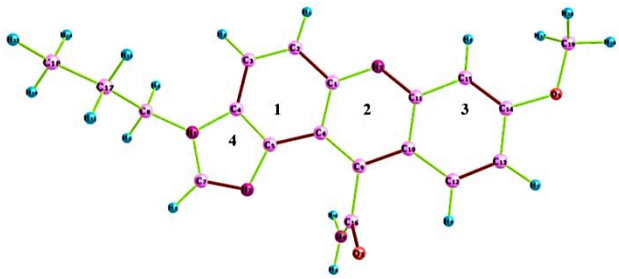

Figure 1. Optimized structure of 8-methoxy-3-propyl-3*H*-imidazo[4,5-*a*] acridine-11-carbonitrile[5].

The SwissParam web server [26] was utilized to compute the force field parameters of the 5. The steepest descent approach was used to minimize energy [27] in order to remove the fundamental kinetic energy from each simulation box as well as to remove any incorrect connections between the atoms. In both the NVT and NPT ensembles, each simulation box attained two-stage equilibrium. At this point, the equilibration period was set to 5ns with a time step of 2fs. At last,

molecular dynamics was carried out by solving the Newton's second principle for 100ns with a time step of 2fs. Electrostatic interactions were calculated using the PME technique [28, 29]. LINCS algorithm [30] was used to strengthen the chemical interactions between the protein's atoms and SETTLE algorithm [31, 32] for solvent molecules. To keep the temperature and pressure constant throughout the simulations, in all equilibration phases and molecular dynamics simulations, V-rescale and Nose-Hoover thermostats were used to couple with system components [33, 34].

RESULTS AND DISCUSSION

As shown in Figure 2, 1-propyl-5-nitro-1*H*-benzoimidazole (**2**) as precursor was prepared by the reaction of 5-nitro-1*H*-benzimidazole (1) reaction with propyl bromide in DMF/KOH at rt [17]. In the next step, the compound 2's nucleophilic replacement of hydrogen with 2-(4- methoxyphenyl) acetonitrile (3) led to the formation of 3*H*-imidazo[4,5-*a*] acridine-11-carbonitrile 4 in MeOH/KOH solution. Finally, hydrolyze of the CN group of compounds **4** in acidic media, produced new amide **5** in high yield.

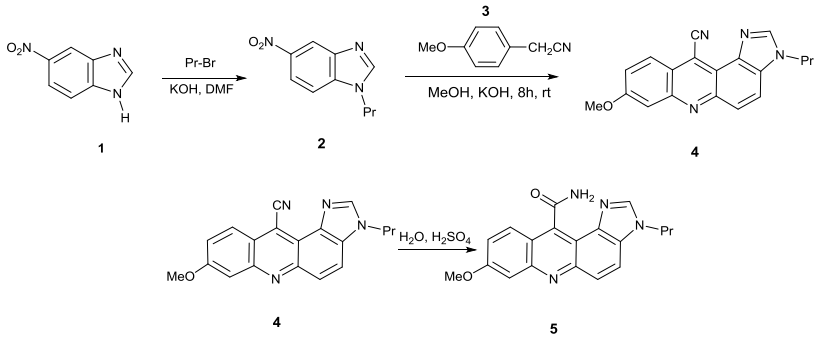

Figure 2. Synthesis of the new compound 5.

Analytical and spectroscopic data validated the structure of novel amide 5. (See Experimental section).

For the simulations' sampling, free energy landscape (FEL) analysis method is the case [35]. The three major steps of FEL analysis are as follows: *i)* Calculations of the protein's radius of gyration (Rg) and the root-mean-square-deviation (RMSD) *ii)* determining the existence of a protein structure in each matching value of RMSD and Rg and *iii)* computation of configurations' free energy based on presence probability values. The result of FEL analysis has shown in 3D diagrams in Figure 3.

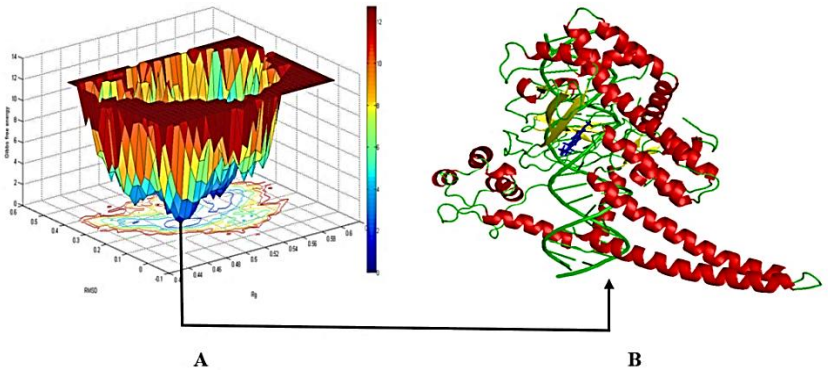

A B

Figure 3. A) diagram of FEL analysis, B) the structure of topoisomerase sampled from simulated system in presence of 5.

In this figure, the blue color represents the smallest areas of unrestricted energy. These figures indicate that simulated system has local minimum, meaning that protein in the presence of 5 has configurated stable. The sampling complex structure derived from the molecular dynamic simulation, which corresponds to the local minimum, is shown in Figure 3. The compound 5 in this figure is shown in blue. According to this figure, compound 5 is located between the strands of the nucleic acid and interacts with the protein. For closer examination, the binding pocket of compound 5 was obtained. In Figure 4, the binding site of the compound 5, along with the effective residues in the interaction of the 5 with the *Topo-I* is shown.

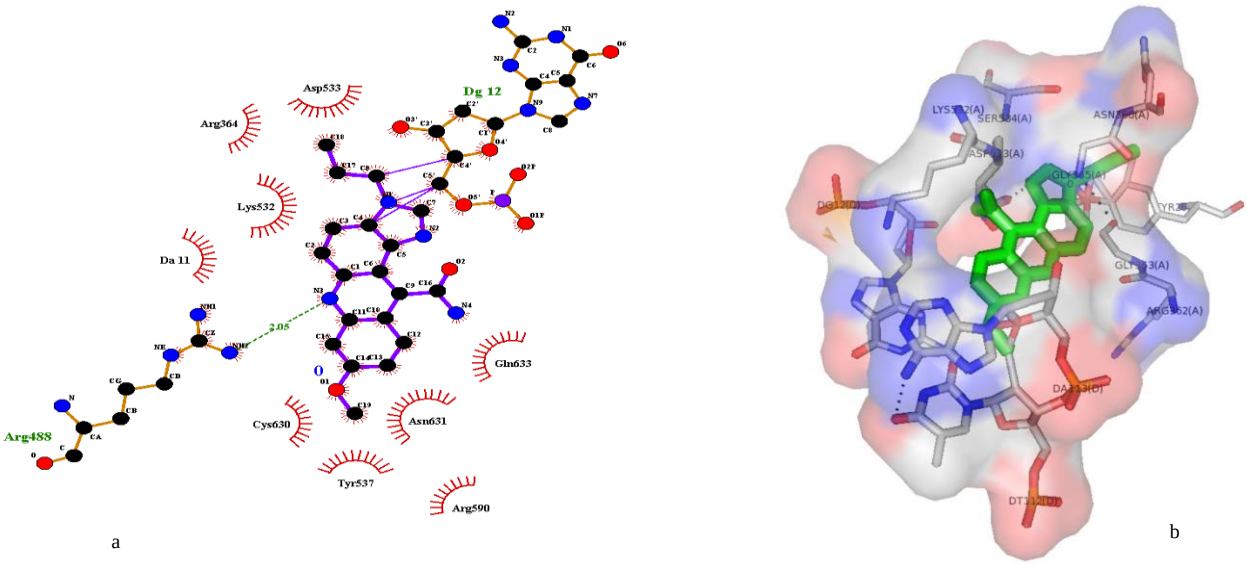

Figure 4. schematic representation of the interaction's ligand in binding site of topoisomerase. It was done using (a) LigPlus program (b) Pymol.

This figure is derived from the LigPlot^{+} software [36]. According to the figure, Arg364, Lys532, Asp533, Tyr537, Arg590, Cys630, Asn631, Gln633 and Adenine11 interact with the 5 by hydrophobic interactions. Also, Arg488 and Adenine12 interact with the compound **5** by hydrogen bond interactions. From these residues, Arg488 and Arg590 are directly in the operating place of *Topo-I*. Also, residues Cys630, Asn631 and Gln633 are in the vicinity of His632, which is located in the active place of the *Topo-I* [37,20]. According to the name of the compound **5** rings mentioned in Figure 1 with numbers 1 to 4, it can be seen that rings 4 and 3 have the most interaction with the enzyme, and ring 2 has the least interaction with the enzyme. To explain this, the HOMA index (Harmonic Oscillator Model for Aromaticity) was calculated [38,39]. The HOMA index was calculated from the following equation:

$$HOMA = 1 - \sum_i \frac{\alpha_{i,j}}{N}\left(R_{Ref} - R_{i,j}\right)^2 \qquad (1)$$

Where j represents the atoms adjacent to each other i, denotes the atom next to atom i, R_{Ref} and α are constants that have already been determined and given in original references [38-40] for each atom-pair type and N is the atoms' total number.

In case of HOMA = 0, the ring is entirely non-aromatic. If HOMA = 1, it means that each bond's length is the same as the optimal value R_{Ref} ,therefore, the ring is entirely aromatic.

If HOMA takes a substantial negative value, then the e ring has an anti-aromatic quality about it. For the calculation of HOMA, The MULTIWFN was used [41]. The values of the HOMA index and the contribution of each bond in this index are listed in Table 1.

Table 1. the values of the HOMA index and the contribution of every bond in this index

Ring	Atom pair	contribution	bond length (A^o)	HOMA
1				0.604068
	C1…C2	-0.124530	1.441846	
	C2…C3	-0.061987	1.350010	
	C3…C4	-0.050539	1.422303	
	C4…C5	-0.005521	1.376663	
	C5…C6	-0.083590	1.432116	
	C6…C1	-0.069766	1.428303	
2				0.874781
	C1…C6	-0.69766	1.428303	
	C6…C11	-0.000965	1.392739	
	C11-C12	-0.005447	1.399262	
	C12…C13	-0.048536	1.421616	
	C13…N14	-0.000000	1.334157	
	N14…C1	-0.000504	1.328312	
3				-97.629933
	C12…C13	-0.048536	1.421616	
	C13…C15	-48.269560	2.448120	
	C15…C16	-0.064305	1.349306	
	C16…C17	-0.070965	1.428648	
	C17…C18	-0.051750	1.353288	
	C18…C12	-50.124817	2.468301	
4				-28.915768
	C4…C5	-0.006625	1.376663	
	C5...N7	-14.066178	2.201203	
	N7…C8	-0.019558	1.366337	
	C8…N9	-0.019351	1.301835	
	N9…C4	-15.804056	2.253215	

Regarding the values of Table 1, rings 2 and 3 are aromatic and the rings 1 and 4 are anti-aromatic. Therefore, the reactivity of rings 1 and 4 is more than the reactivity of rings 2 and 3. To determine the affinities of binding between the compound **5** and binding pocket residues of the *Topo-I*, the MMPBSA algorithm, provided by Kollman et al., was utilized [42, 43]. The free energy is calculated using this method:

$$G = E_{bnd} + E_{el} + E_{vdW} + G_{pol} + G_{np} - TS \qquad (2)$$

Where $E_{bnd}, E_{el}\ and\ E_{vdW}$ are the energies of MM including bonding, bending, and dihedral, electrostatic

energy and interactions of van der Waals, respectively; G_{pol} and G_{np} are polar and nonpolar free energies of solvation, obtained using the generalized Born and solvent accessible surface methods, respectively. The last term in Eq. 2, where T denotes temperature and S denotes entropy, is the result of a normal mode (NM) analysis. The share of the residues to the binding energy of *Topo-I* with compound 5 is depicted in Figure 5.

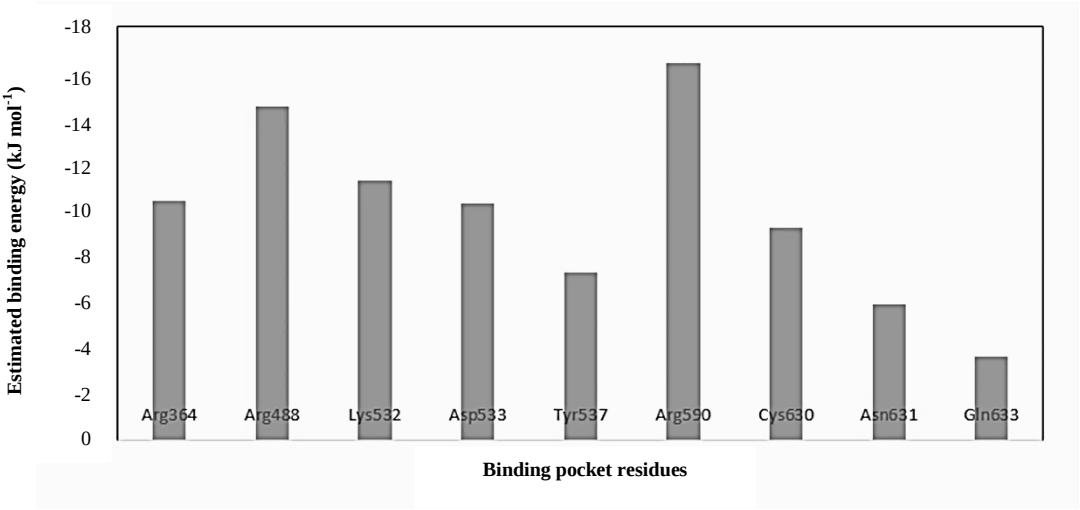

Figure 5. The share of the residues to the energy that binds *Topo-I* with compound 5.

According to the figure, compound 5 affinity to charged residues is higher than un-charged residues. In such a way, the free energy of binding to the Arg residues is greater than the rest of the residues. In summary, a new derivative based on acridine and imidazole was synthesized. The molecular dynamics was used to study of the interaction of this new derivative with topoisomerase enzyme. The calculations showed that the new substance has inhibitory properties for the topoisomerase enzyme.

ACKNOWLEDGEMENTS

We would like to express our sincere gratitude to Research Office, Mashhad Branch, Islamic Azad University, Mashhad-Iran, for financial support of this work.

Conflict of interests

The Authors declare that there is no conflict of interest.

REFERNCES

1. Abd-Allah O., Abdelhamid A., Mohamed S., 2015. Synthesis and Anti-inflammatory Study of Novel N-substituted Hydro-acridine-1, 8-diones and Bis-hexahydroacridine-1, 8-dione Derivatives. Med Chem, S2:004.

2. Mallu L., Thirumalai D., Asharani I.V., 2017. One-pot cascade synthesis and in vitro evaluation of anti-inflammatory and antidiabetic activities of S methylphenyl substituted acridine- 1, 8- diones. Chemical Biology & Drug Design. 90(4), 520-526.

3. Daghigh L.R., Pordel M., Davoodnia A., Jajarmi M., 2015. Synthesis, antiviral, and cytotoxic investigation of imidazo [4, 5-a] acridones. Medicinal Chemistry Research. 24(11), 3912-3919.

4. Kaya M., Yıldırır Y., Çelik G.Y., 2015. Synthesis, characterization, and in vitro antimicrobial and antifungal activity of novel acridines. Pharmaceutical Chemistry Journal. 48(11), 722-726.

5. Nowak K., 2017. Chemical structures and biological activities of bis-and tetrakis-acridine derivatives: A review. Journal of Molecular Structure. 1146, 562-570.

6. Fahrenholtz C.D., Ding S., Bernish B.W., Wright M.L., Zheng Y., Yang M., Yao X., Donati G.L., Gross M.D., Bierbach U., 2016. Design and cellular studies of a carbon nanotube-based delivery system for a hybrid platinum-acridine anticancer agent. Journal of Inorganic Biochemistry. 165, 170-180.

7. Yu Z., Han M., Cowan J.A., 2015. Toward the Design of a Catalytic Metallodrug: Selective Cleavage of G Quadruplex Telomeric DNA by an Anticancer Copper–

Acridine–ATCUN Complex. Angewandte Chemie. 127(6), 1921-1925.

8. Hu Y., Shen Y., Wu X., Tu X., Wang G.X., 2018. Synthesis and biological evaluation of coumarin derivatives containing imidazole skeleton as potential antibacterial agents. European Journal of Medicinal Chemistry. 143, 958-969.

9. Shankar B., Jalapathi P., Valeru A., Kumar A.K., Saikrishna B., rao Kudle K., 2017. Synthesis and biological evaluation of new 2-(6-alkyl-pyrazin-2-yl)-1H-benz [d] imidazoles as potent anti-inflammatory and antioxidant agents. Medicinal Chemistry Research. 26(9), 1835-1846.

10. Posfai D., Eubanks A.L., Keim A.I., Lu K.Y., Wang G. Z., Hughes P.F., Kato N., Haystead T. A., Derbyshire E.R., 2018. Identification of Hsp90 inhibitors with anti-Plasmodium activity. Antimicrobial Agents and Chemotherapy. 62(4).

11. Corcoran J., Lange A., Cumming R.I., Owen S.F., Ball J.S., Tyler C.R., Winter M.J., 2014. Bioavailability of the imidazole antifungal agent clotrimazole and its effects on key biotransformation genes in the common carp (*Cyprinus carpio*). Aquatic Toxicology. 152, 57-65.

12. Ebadian B., Fathi A., Savoj M., 2021. In Vitro Evaluation of the Effect of Different Luting Cements and Tooth Preparation Angle on the Microleakage of Zirconia Crowns. International Journal of Dentistry. 8461579.

13. Zechiedrich E.L., Osheroff N., 1990. Eukaryotic topoisomerases recognize nucleic acid topology by preferentially interacting with DNA crossovers, The EMBO Journal. 9(13), 4555-4562.

14. Abolhasani M., Givehchian P., Fathi A., Goudarzi S., 2021. Relationship of Life Satisfaction and Satisfaction with Fixed Implant-Supported Prostheses in the Elderly. Journal of Iranian Dental Association. 33(1), 17-21

15. Champoux J.J., 2001. DNA topoisomerases: structure, function, and mechanism. Annual Review of Biochemistry. 70(1), 369-413.

16. Khalil M.S., Ebrahim H.A., Pasalar P., Yaghmaei P., Hayati R.N., 2012. Reflection on design and testing of pancreatic alpha-amylase inhibitors: an in silico comparison between rat and rabbit enzyme models, DARU Journal of Pharmaceutical Science. 20,77

17. Preston P.N., 1981Benzimidazoles and Cogeneric Tricyclic Compounds, Volume 40(1). Wiley: New Jersey,.

18. Maroofi V., Pordel M., Chegini H., Ramezani S., 2015. Synthesis, Spectral Studies and Quantum-Chemical Investigations on the Powerful Fluorophores: Imidazo [4, 5-a] acridines. Journal of Fluorescence. 25(5), 1235-1243.

19. Fathi A., Giti R., Farzin M., 2018. How different influential factors affect the color and translucency of Y-ZTP: A review of the literature. Annals of Dental Specialty. 6(3), 338-341.

20. Stewart L., Redinbo M.R., Qiu X., Hol W.G., Champoux J.J., 1998. A model for the mechanism of human topoisomerase I. Science. 279(5356), 1534-1541.

21. Chillemi G., Redinbo M., Bruselles A., Desideri A., 2004. Role of the linker domain and the 203–214 N-terminal residues in the human topoisomerase I DNA complex dynamics. Biophysical Journal. 87(6), 4087-4097.

22. Fathi A., Farzin M., Giti R., Kalantari M.H., 2019. Effects of number of firings and veneer thickness on the color and translucency of 2 different zirconia-based ceramic systems. The Journal of Prosthetic Dentistry. 122(6), 565-571.

23. Afshar m., Ranjineh K.R., Ahmadi R., Nakhaei M.M., 2021. In Silico Adsorption of Lomustin anticancer drug on the surface of Boron Nitride nanotube. Chem Rev Lett. 4, 178-184.

24. Ghasemi E., Fathi A. H., Parvizinia S., 2019. Effect of three disinfectants on dimensional changes of different impression materials. Journal of Iranian Dental Association. 31(3), 169-176.

25. Schmidt M.W., Baldridge K. K., Boatz J. A., Elbert S. T., Gordon M. S., Jensen J. H., Koseki S., Matsunaga N., Nguyen K. A., Su S., 1993. General atomic and molecular electronic structure system. Journal of Computational Chemistry. 14(11), 1347-1363.

26. Zoete V., Cuendet M.A., Grosdidier A., Michielin O., 2011. SwissParam: a fast force field generation tool for small organic molecules. Journal of Computational Chemistry. 32(11), 2359-2368.

27. Luenberger D.G., Ye Y., 1984. Linear and nonlinear programming., Springer: New York.

28. Essmann U., Perera L., Berkowitz M.L., Darden T.,

Lee H., Pedersen L.G., 1995. A smooth particle mesh Ewald method. The Journal of Chemical Physics. 103(19), 8577-8593.

29. Kaviani R., 2022. Use Bioethanol as a Clean and Cost-Effective Fuel. Journal of Engineering in Industrial Research. 3(2), 147-152.

30. Hess B., Bekker H., Berendsen H.J., Fraaije J.G., 1997. LINCS: a linear constraint solver for molecular simulations. Journal of Computational Chemistry. 18(12), 1463-1472.

31. Jedariforoughi A., 2022. Bioreactor based cancer therapy. Doctmedico Journal. 2(2), 201-206.

32. Miyamoto S., Kollman P.A., 1992. SETTLE: an analytical version of the SHAKE and RATTLE algorithm for rigid water models. Journal of Computational Chemistry. 13(8), 952-962.

33. Bussi G., Donadio D., Parrinello M., 2007. Canonical sampling through velocity rescaling. The Journal of chemical physic. 126(1), 014101.

34. Monirifard R., Abolhasani M., Tahani B., Fathi A., Choobdaran A., 2019. Relationship of Personality Traits and Patient Satisfaction with Fixed Implant Prosthodontic Treatments. Journal of Iranian Dental Association. 31(4), 182-188.

35. Lei H., Wu C., Liu H., Duan Y., 2007. Folding free-energy landscape of villin headpiece subdomain from molecular dynamics simulations. Proceedings of the National Academy of Sciences. 104(12), 4925-4930.

36. Wallace A.C., Laskowski R.A., Thornton J.M., 1995. LIGPLOT: a program to generate schematic diagrams of protein-ligand interactions. Protein Engineering, Design and Selection. 8(2), 127-134.

37. Shirzadi P., Vaziri P., Lo Han K., Johnson A., 2022. Investigating the Impact of Energy on Iran's National Security. Journal of Engineering in Industrial Research. 3(2), 161-167.

38. Kruszewski J., Krygowski T., 1972. Definition of aromaticity basing on the harmonic oscillator model. Tetrahedron Letters. 13(36), 3839-3842.

39. Krygowski T.M., 1993. Crystallographic studies of inter-and intramolecular interactions reflected in aromatic character of pi-electron systems. Journal of Chemical Information and Computer sciences. 33(1), 70-78.

40. Shirzadi P., 2022. Optimization and Simulation of Process Unit in the Chemical Industry. Journal of Engineering in Industrial Research. 3(2), 153-160.

41. Lu T., Chen F., 2012. Multiwfn: a multifunctional wavefunction analyzer. Journal of Computational Chemistry. 33(5), 580-592.

42. Kollman P.A., Massova I., Reyes C., Kuhn B., Huo S., Chong L., Lee M., Lee T., Duan Y., Wang W., 2000. Calculating structures and free energies of complex molecules: combining molecular mechanics and continuum models. Accounts of Chemical Research. 33(12), 889-897.

43. Kumari R., Kumar R., Consortium O.S.D.D., Lynn A., 2014. g_mmpbsa A GROMACS tool for high-throughput MM-PBSA calculations. Journal of Chemical Information and Modeling. 54(7), 1951-1962.